Slow drag in polydisperse granular mixtures under high pressure

Fuping Zhou and Suresh G. Advani
Department of Mechanical Engineering and Center for Composite Materials, University of Delaware, Newark, Delaware 19716, USA

Eric D. Wetzel
Army Research Laboratory Aberdeen Proving Ground, Maryland 21005, USA

(Received 13 September 2004; revised manuscript received 19 April 2005; published 23 June 2005)

The behavior of polydisperse granular materials, composed of mixtures of particles of different sizes, is studied under conditions of high pressure and confinement. Two types of experiments are performed. In the first type, granular mixtures are compressed, with the resulting force-displacement curve used to calculate density and volume modulus. In the second set of experiments, the drag force is measured by pulling a cylinder, horizontally, through a compressed granular mixture. The density, volume modulus, and drag forces for the mixtures are quantified in terms of the mixture composition. The results show that the behavior of these mixtures depends strongly on the mass fractions of the different sized particles, with density, volume modulus, and drag force all reaching values significantly higher than observed in the monodisperse granular materials. Furthermore, the trends for density and drag force show strong correlation, suggesting that drag resistance of confined granular media could be directly related to packing effects. These results should prove useful in understanding the physics of drag in granular materials under high pressure, such as ballistic penetration of soils or ceramic armors.

DOI: 10.1103/PhysRevE.71.061304 PACS number(s): 83.80.Fg, 45.70.−n, 62.20.Dc, 81.05.Rm

I. INTRODUCTION

Many industrial and natural processes involve granular flows, which can include mixing, advection, or compaction of granular materials. To better understand these processes, a number of researchers have investigated the flow behavior of granular materials. These experiments include shear flows [1–4] and flow past an immersed cylinder [5–10]. These experiments, however, typically involve low pressures and free boundaries; therefore, the flow resistance is relatively low.

In contrast, many processes involve the flow of confined granular materials under high pressures. Of particular interest are the granular flows that take place during the ballistic impact of ceramic armors [11,12]. Previous experiments have shown that drag flow in confined, pressured granular beds is significantly different from drag flow in unconfined granular materials [13,14]. Specifically, the drag forces for confined flow are much higher than unconfined flow and scale linearly with compaction pressure. Additionally, the drag force in confined flow is strongly dependent on the granule size, increasing as granule size increases.

In this paper, we perform experiments to explore the behavior of granular mixtures under high pressures. These mixtures are composed of three different granule sizes, combined in various proportions. In the first set of experiments, the effective density of a packed granular mixture is measured as a function of mass fraction. In the second set, the drag force for flow past a cylinder is used to characterize the viscouslike properties of a confined and pressurized granular mixture as a function of mass fraction. These experiments will expand our understanding of the flow behavior of confined granular media under high pressures and will enable the formulation of constitutive models or the extension of existing models (e.g., [15–18]).

Some experimental and theoretical investigations have been performed to determine the effect of particle size distribution on packing efficiency. These studies [19–25] generally show that polydisperse packing leads to the highest possible mixture densities.

II. EXPERIMENTS

A. Materials

Mixtures of white aluminum oxide granules (AGSCO Corporation, Hasbrouch Heights, NJ) of different sizes were used in the experiments. The granules were mechanically mixed for about 10 min prior to loading them into the compression and drag chambers to ensure good mixing. Their average sizes along with the minimum and maximum values are summarized in Table I. The densities of these particles are 3.94, 3.93, and 3.92 g/cm^3 for the coarse, medium, and fine granule sizes, respectively [14]. Three different types of binary mixtures were studied: coarse-fine (cf), coarse-medium (cm), and medium-fine (mf) mixtures. For each type of mixture, the relative amount of the two particle sizes was systematically varied. We define the mass fraction x for these binary mixtures as the mass-based proportion of the larger particles in the mixture. Additionally, a few experiments

TABLE I. Average, maximum, and minimum granule sizes (D_g) for the granular materials investigated, as reported by the manufacturer.

	Ave. size (μm)	Max. size (μm)	Min. size (μm)
Coarse granules	1092	1650	787
Medium granules	483	762	305
Fine granules	165	292	102

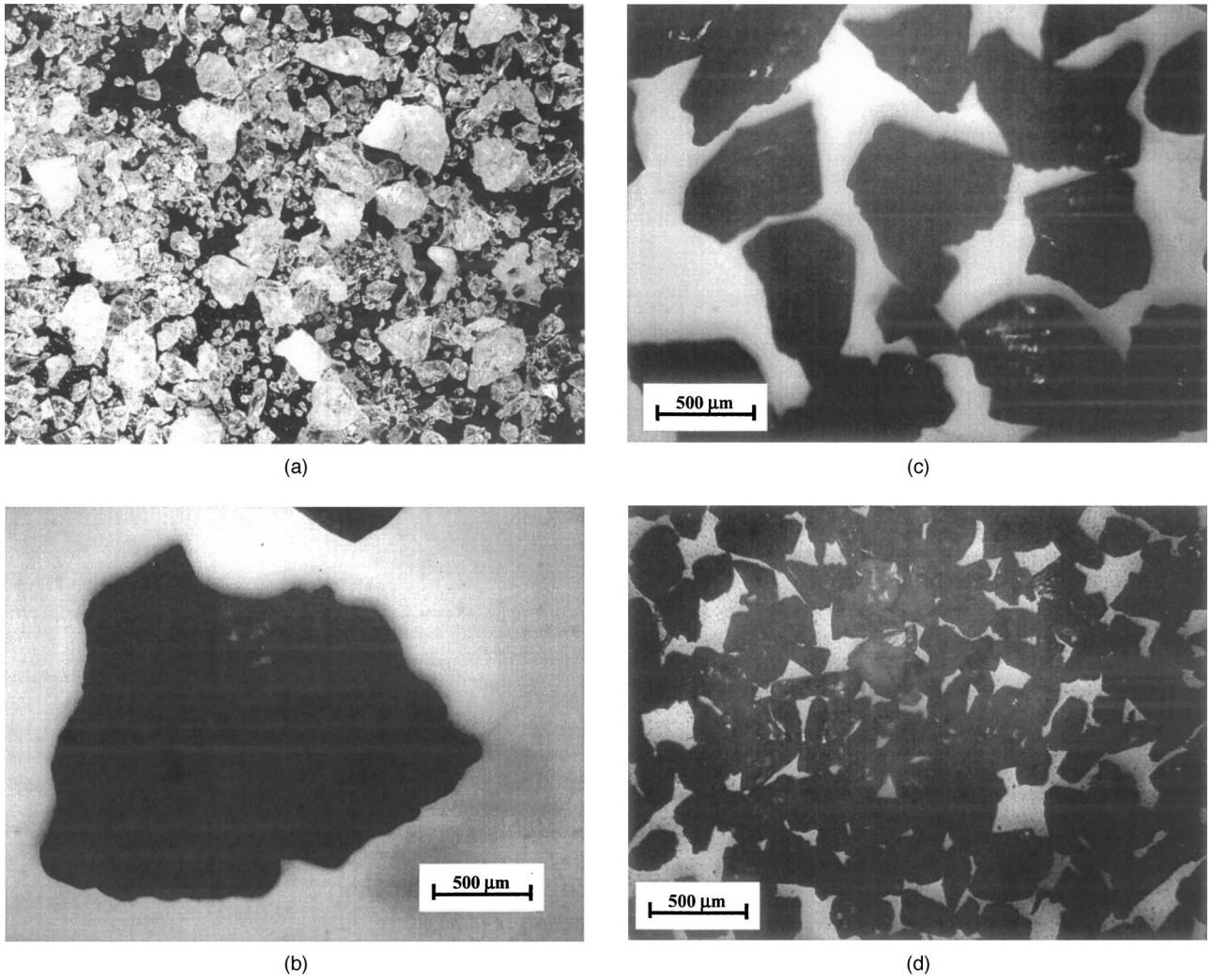

FIG. 1. Images of granules. (a) mixture of coarse-medium-fine granules, (b) coarse granules, (c) medium granules, and (d) fine granules. Note that (b)–(d) have the same magnification.

were performed using a ternary blend of each of the three particle sizes. Figure 1 shows the relative size of coarse, medium, and fine granules in the mixture.

B. Compression experiments

To characterize the compression behavior of granular mixtures under high pressure, compression experiments were conducted as described in [14]. Well-mixed granular mixtures of known mass and mass fraction were placed in the steel containment cylinder and compressed using an Instron mechanical tester. The granular mixture was agitated during filling of the chamber to improve packing. In all cases, the compression rate (linear speed of the chamber lid) was 0.5 mm/s, and the reported data represents the average of three experiments. The containment cylinder has an internal diameter (D_c) of 38.1 mm and a maximum chamber height of 38.1 mm. The compression force (F_c) and cylinder diameter can be used to calculate the applied pressure p

$$p = \frac{4F_c}{\pi D_c^2}, \tag{1}$$

while the effective density ρ of the granular bed can be calculated based on the mass of the granules m and the instantaneous height of the granular materials h:

$$\rho = \frac{4m}{\pi D_c^2 h}. \tag{2}$$

The rate of densification can be characterized in terms of a volume modulus K, which includes the effects of both reorganization of the granular bed and bulk modulus of the individual granules. Figure 2 shows that, under high pressure, the granular density approaches a linear dependence on the confinement pressure. The volume modulus [26] (or modulus of volume expansion [27]) for these mixtures can then be characterized as

$$\rho = kp + \rho_o, \tag{3}$$

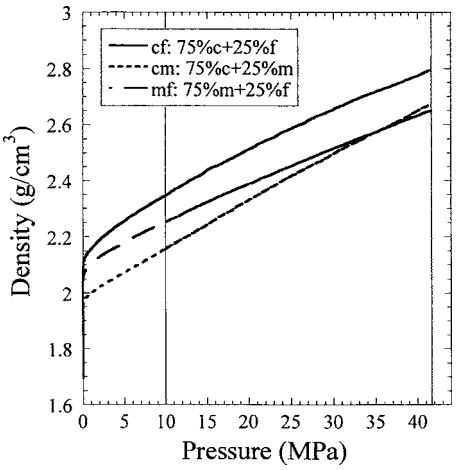

FIG. 2. Typical compression results. The vertical lines indicate the pressure range over which the volume modulus is calculated.

$$e = \frac{dh}{h}, \tag{4}$$

$$K = \frac{dp}{de}, \tag{5}$$

or

$$K = \frac{\rho}{k}, \tag{6}$$

where ρ is the instantaneous density, ρ_o is the initial (uncompressed) density, e is compression strain, and k is the slope of pressure-density curve of the granular mixture. In all cases, the volume modulus is calculated based on a best-fit line over the range of $p=10$–41.6 MPa.

C. Drag-force experiments

To characterize the flow behavior of the pressurized granular mixtures, drag experiments were performed as described in [14]. Figure 8 in [14] shows micrographs of the granules before and after the drag experiments. One can see many particles after the drag experiment that are orders of magnitude smaller than the granule shapes and sizes before and after the experiment. In fact, these particles are so small that the average granule shape and size is not affected by the experiment. So granule fracture does not play an important role, nor is it a significant factor in contribution toward the drag force. The granular mixtures were placed in a 101.6 mm diam cylindrical chamber to a height of 120 mm, and precompacted to a known pressure. The lid was then mechanically secured to maintain a constant chamber volume during the experiment. An immersed horizontal cylindrical rod attached to a long shaft was then pulled through the compacted mixture using an Instron mechanical tester, which records the drag force as a function of cylinder displacement. Figure 3 schematically shows the experimental setup.

The method by which the granules are packed into the containment cylinder has a noticeable influence on the initial void distribution in the packed bed, which, in turn, can strongly influence the drag behavior [28]. To minimize this effect, the granular mixture was stirred and agitated during filling to achieve maximum packing. New, untested granules were used for each experiment.

All experiments used a cylindrical rod diameter $D=6.35$ mm, a rod length $L=49.53$ mm, a compaction pressure $p=5.63$ MPa, and a drag velocity $v=0.5$ mm/s. The drag force F for a given measurement is defined as the average value of the drag force measured between 10 and 30 mm of displacement (shown later in Fig. 8), and each point in the figure represents the average of three experiments.

III. RESULTS

A. Compression experiments

Figure 4 shows the measured densities at $p=41.6$ MPa as a function of mass fraction for the compression experiments. All standard deviations for density are $<0.7\%$ and the average is $\sim 0.26\%$. In general, density depends strongly on mixture composition. However, for each type of mixture, the density approaches a maximum when the mass percentage of larger granules is ~ 70–80%. Note that, for all experiments, mixture density does not approach the limiting density of the granules themselves (3.9 g/cm^3). In general, the highest densities are noted for the coarse-fine mixture.

Figure 5 shows the volume modulus as a function of mass fraction. All standard deviations for volume modulus are $<3.0\%$ and the average is $\sim 1.3\%$. The volume modulus reaches a maximum when the mass fraction of the larger granules is $\sim 50\%$ for medium-fine and coarse-fine mixtures. For coarse-medium mixtures, the volume modulus reaches a

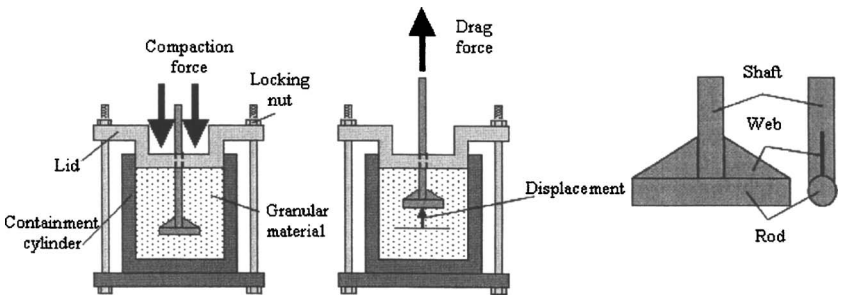

FIG. 3. Schematic of the device used for drag experiments: (a) application of compaction pressure, (b) dragging cylinder through granular bed, and (c) detailed view of the cylinder.

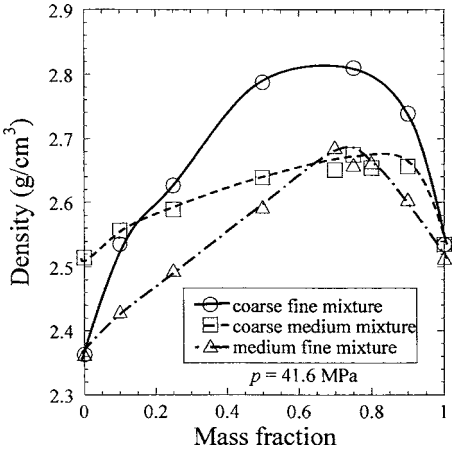

FIG. 4. Density of different mixtures at p=41.6 MPa as a function of mass fraction (lines are guides to the eye).

maximum when mass fraction of the coarse granules is about 25%.

Figure 6 summarizes the compression behavior of the ternary mixtures and some of the binary and single-component mixtures. Densities are given at fixed pressures of 41.6 MPa and at effective "drag pressures" of $p=F/DL$, where DL is the frontal area of the rod and F is the drag force measured for each mixture. These drag pressures range from 8.9 to 22.6 MPa. In all cases, two- and three-component mixtures reach higher density than those of pure granules. The densities at p=41.6 MPa are always higher than the densities at effective drag pressures.

Figure 7 shows volume modulus of single-component, binary, and ternary mixtures, at both p=41.6 MPa and $p=F/DL$. Unlike density, the volume modulus for some of the single-component systems is higher than that observed in some of the mixed systems. However, the lowest volume modulus is observed in a single-component system (coarse), and the highest volume modulus is observed in a ternary mixture.

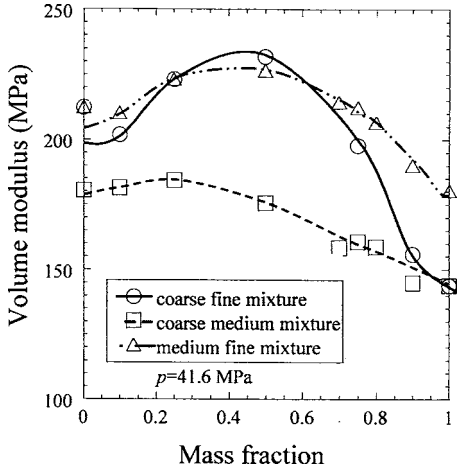

FIG. 5. Volume modulus of mixtures at p=41.6 MPa (lines are guides to the eye).

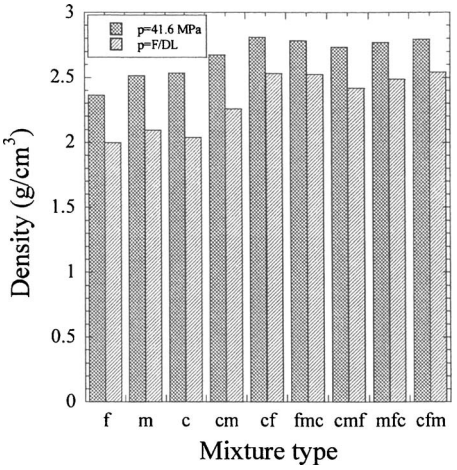

FIG. 6. Density of granular mixtures at p=41.6 MPa (f: fine; m: medium; c: coarse; cm: 75%c+25%m; cf: 75%c+25%f; fmc: 33.3%f+33.3%m+33.3%c; cmf: 75%c+18.75%m+6.25%f; mfc: 12.5%m+12.5%f+75%c; and cfm: 75%c+18.75%f +6.25%m).

B. Drag-force experiments

Figure 8 shows the general drag behavior observed for the granular mixture experiments. As the rod is pulled through the granular mixture, an initial rise in drag force is followed by a relatively constant drag-force region. Figure 8 also shows the region chosen for calculating average drag values (10–30 mm). This choice is somewhat arbitrary and attempts to capture a typical steady drag-force value [14]. All standard deviations for drag force are $<$11% and the average is $\sim$5.1%.

Figure 9(a) shows the drag force as a function of mass fraction. Drag force varies considerably with composition, approaching a maximum when the mass percentage of larger granules is $\sim$70–80%. This trend is very similar to the variation in density with mass fraction in Fig. 4, which also reaches a peak value between 70 and 80%. In contrast, the

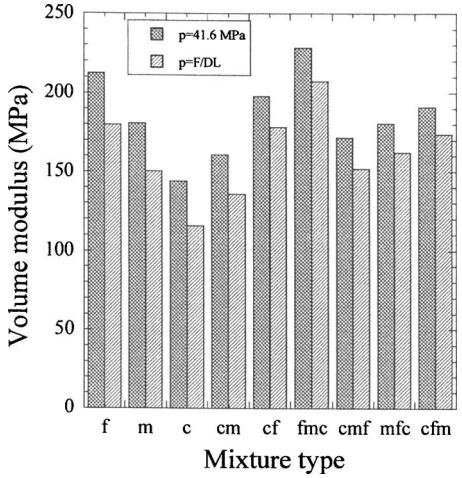

FIG. 7. Volume modulus of granular mixtures at $p=F/DL$ and p=41.6 MPa. Mixture compositions and labels are consistent with those of Fig. 6.

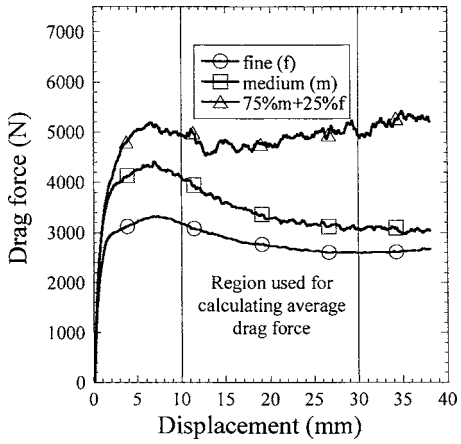

FIG. 8. Generalized behavior of drag force in granular mixture.

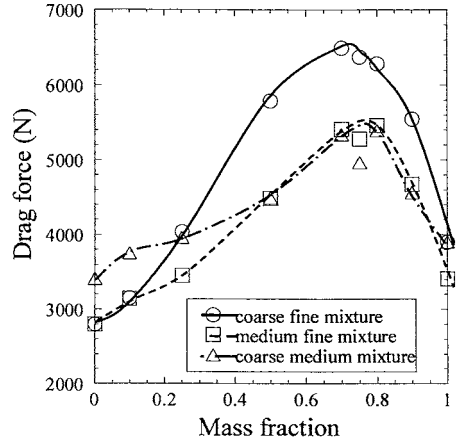

(a)

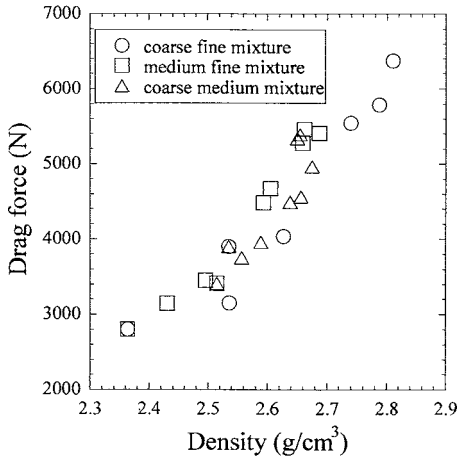

(b)

FIG. 9. Drag force for binary mixtures (lines are guides to the eye): (a) drag force as a function of mass fraction and (b) drag force as a function of density at $p=41.6$ MPa.

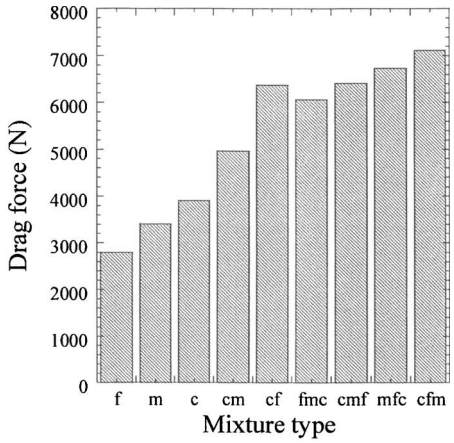

(a)

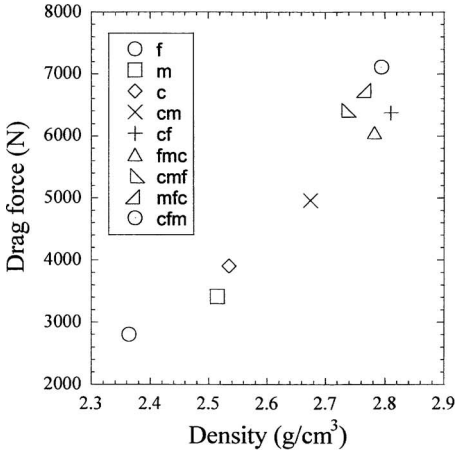

(b)

FIG. 10. (a) Drag force for single-component, binary, and ternary mixtures and (b) drag force as a function of density at $p=41.6$ MPa. Mixture compositions and labels are consistent with those of Fig. 6.

volume modulus reached a maximum when the percentage of larger granules was ~30–50%. To further demonstrate the linkage between density and drag force, Fig. 9(b) plots the drag force for each mixture versus its density at $p=41.6$ MPa. All the drag-force results appear to collapse onto a single curve, perhaps suggesting that mixture density alone determines drag behavior.

Figure 10(a) compares the drag-force values of single-component, binary, and ternary mixtures. Note that drag force generally increases as the number of components increase. These trends are consistent with the density values reported in Fig. 6. Figure 10(b) plots the drag force values as a function of the mixture densities at $p=41.6$ MPa, again showing that drag force scales strongly with mixture density.

IV. DISCUSSION

The drag experiments and compression experiments show similar trends with respect to mass fraction in the polydis-

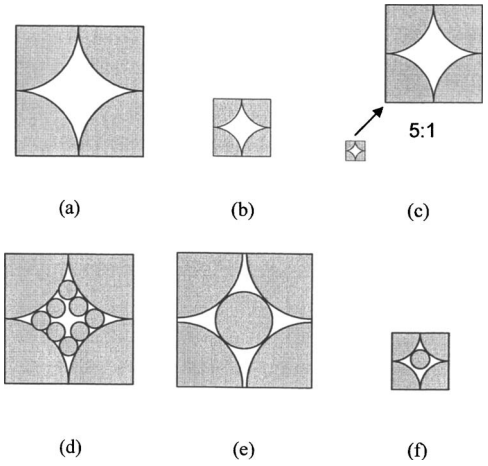

FIG. 11. Unit cell models containing spherical particles to evaluate packing fraction. Top row: monodisperse spheres [coarse (a), medium (b), and fine (c)]. Bottom row: (from left to right) Coarse-fine (d), coarse-medium (e), and medium-fine mixtures (f).

perse mixture. The peak drag force occurs when the particles are optimally packed, that is when the granular material has highest density and lowest free volume. It is reasonable to hypothesize that the peak drag force is due to minimum free volume in the system. With more free volume available, it is much easier for the system to reconfigure itself. In this section, further evidence of this effect is provided by calculating the maximum effective density as a function of mixture composition, for the particular granular sizes used in our experiments.

As a first-order approximation, we can assume all granules to be spherical and each type of granule (fine, medium, or coarse) to have a diameter equal to the reported average particle size for our mixtures. These diameters are $D_f = 165\ \mu$m, $D_m = 483\ \mu$m, and $D_c = 1092\ \mu$m for the fine, medium, and coarse granules, respectively. To further simplify our analysis, we will only calculate two-dimensional (2D) packing efficiencies. These approximations, of course, neglect the three-dimensional (3D), polydisperse, and nonspherical nature of our actual granules, and therefore will only allow for qualitative comparisons.

For our calculations, we will assume simple (square) packing. Figures 11(a)–11(c) show unit cells for pure coarse, fine, and medium particles. For these cases, the effective granular density is $\rho = (\pi/4)\rho_g$, where ρ_g is the density of the individual alumina granules. Assuming $\rho_g = 3.9\ \mathrm{g/cm^3}$, the effective density of the unmixed granular media is $3.06\ \mathrm{g/cm^3}$. Note that our measured peak densities for unmixed particles ranged from 2.4 to 2.5 $\mathrm{g/cm^3}$, indicating that our packing efficiency is well below these theoretical geometries.

Considering binary mixtures, the maximum effective density can be calculated by calculating the maximum number of smaller particles that can fit within a unit cell composed of larger particles. Figures 11(d)–11(f) show these unit cells. For the coarse-fine mixture, eight fine particles can fit inside a simple-packed coarse unit cell. The effective density for this mixture is

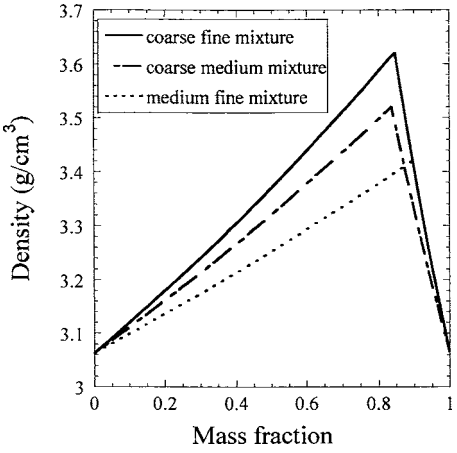

FIG. 12. Theoretical densities for granular mixtures, based on simple 2D packing assumptions.

$$\rho_{\mathrm{cf}} = \frac{\pi}{4}\rho_g[1 + 8(D_f/D_c)^2], \tag{7}$$

at mass fraction of

$$x_{\mathrm{cf}} = [1 + 8(D_f/D_c)^2]^{-1}. \tag{8}$$

For the coarse-medium mixture at maximum packing, the coarse simple lattice requires some spacing between particles to allow room for the medium particle at the center of the unit cell. The effective density is then

$$\rho_{\mathrm{cm}} = \frac{\pi}{2}\rho_g \frac{D_c^2 + D_m^2}{(D_c + D_m)^2}, \tag{9}$$

at a mass fraction of

$$x_{\mathrm{cm}} = [1 + (D_m/D_c)^2]^{-1}. \tag{10}$$

For the medium-fine mixture, the fine particle fits at the center of a simple packed medium unit lattice. The maximum effective density for this mixture is then

$$\rho_{\mathrm{mf}} = \frac{\pi}{4}\rho_g[1 + (D_f/D_m)^2], \tag{11}$$

at a mass fraction of

$$x_{\mathrm{mf}} = [1 + (D_f/D_m)^2]^{-1}. \tag{12}$$

Numerically, for our granule sizes and densities, the maximum effective densities for each mixture are $\rho_{\mathrm{cf}} = 3.62\ \mathrm{g/cm^3}$, $\rho_{\mathrm{cm}} = 3.52\ \mathrm{g/cm^3}$, and $\rho_{\mathrm{mf}} = 3.42\ \mathrm{g/cm^3}$, at particle mass fractions of $x_{\mathrm{cf}} = 0.846$, $x_{\mathrm{cm}} = 0.836$, and $x_{\mathrm{mf}} = 0.895$.

For intermediate particle mass fractions, we assume that particles not arranged in these optimally packed binary unit cells will be arranged in simple, single-component unit cells. Therefore, the effective density of the mixture will vary linearly with mass fraction between the pure granular media values and maximum density values. These continuous trends in effective density as a function of mass fraction are shown in Fig. 12. The curves are similar in appearance to our experimentally measured density curves in Fig. 4, although the theoretical density values are, in general, much higher.

Note that both the theoretical and experimental curves show maximums around 80%, with the highest effective densities for the coarse-fine mixture. These same trends follow for the drag-force curves of Fig. 9. These results further suggest that packing effects could be crucial to determining both compaction and flow behavior of pressurized granular media. Note that Santiso and Muller [23] predict similar trends in packing efficiency for binary mixtures of spherical particles.

V. CONCLUSIONS

The experimental investigation of drag flow in pressurized granular mixtures shows that drag force in polydisperse granular systems is higher than in granular material composed of uniformly sized particles. For binary mixtures, drag force is highest when the mass percentage of the larger-sized granules is around 70–80%. These same trends are also observed for effective granular density and correlate less strongly with volume modulus. The experimental results also show that higher density and drag-force values are observed for ternary mixtures, as compared to binary mixtures. It is reasonable to hypothesize that the peak drag force is due to minimum free volume, which makes it difficult for the system to reconfigure itself. Simple unit cell models of particle packing exhibit similar trends as the experimental results, suggesting that packing physics plays an important role in determining the flow resistance of confined, pressurized granular media.

ACKNOWLEDGMENTS

The support of the project from the Army Research Laboratory is gratefully acknowledged. We would also like to thank John Barr for experimental assistance.

[1] J. F. Klausner, D. M. Chen, and R. W. Mei, Powder Technol. **112**, 94 (2000).
[2] G. I. Tardos, M. I. Khan, and D. G. Schaeffer, Phys. Fluids **10**, 335 (1998).
[3] G. Ovarlez, E. Kolb, and E. Clement, Phys. Rev. E **64**, 060302 (2001).
[4] S. Nasuno, A. Kudrolli, and J. P. Gollub, Phys. Rev. Lett. **79**, 949 (1997).
[5] R. Albert, M. A. Pfeifer, A. L. Barabasi, and P. Schiffer, Phys. Rev. Lett. **82**, 205 (1999).
[6] I. Albert, P. Tegzes, R. Albert, J. G. Sample, A. L. Barabasi, T. Vicsek, B. Kahng, and P. Schiffer, Phys. Rev. E **64**, 031307 (2001).
[7] I. Albert, P. Tegzes, B. Kahng, R. Albert, J. G. Sample, M. Pfeifer, A. L. Barabási, T. Vicsek, and P. Schiffer, Phys. Rev. Lett. **84**, 5122 (2000).
[8] B. Kahng, I. Albert, P. Schiffer, and A. L. Barabasi, Phys. Rev. E **64**, 051303 (2001).
[9] I. Albert, J. G. Sample, A. J. Morss, S. Rajagopalan, A. L. Barabasi, and P. Schiffer, Phys. Rev. E **64**, 061303 (2001).
[10] G. D'Anna, Europhys. Lett. **51**, 293 (2000).
[11] D. A. Shockey, A. H. Marchand, S. R. Skaggs, G. E. Cort, M. W. Burkett, and R. Parker, Int. J. Impact Eng. **9**, 263 (1990).
[12] D. R. Curran, L. Seaman, T. Copper, and D. A. Shockey, Int. J. Impact Eng. **13**, 53 (1993).
[13] F. Zhou, S. G. Advani, and E. D. Wetzel, ASME, Materials Division (Publication) MD **98**, 145 (2003).
[14] F. Zhou, S. G. Advani, and E. D. Wetzel, Phys. Rev. E **69**, 061306 (2004).
[15] S. C. Cowin, Acta Mech. **20**, 41 (1974).
[16] M. A. Goodman, and S. C. Cowin, J. Fluid Mech. **45**, 321 (1971).
[17] W. A. M. Brekelmans, Powder Technol. **62**, 21 (1990).
[18] H. S. Kim, S. T. Oh, and J. S. Lee, J. Am. Ceram. Soc. **85**, 2137 (2002).
[19] T. Aste, Phys. Rev. E **53**, 2571 (1996).
[20] N. Brilliantov, Y. A. Andrienko, P. Krapivsky, and J. Kurths, Phys. Rev. Lett. **76**, 4058 (1996).
[21] N. Brilliantov, Y. A. Andriendo, P. Krapivsky, and J. Kurths, Phys. Rev. E **58**, 3530 (1998).
[22] P. S. Dodds and J. S. Weitz, Phys. Rev. E **65**, 056108 (2002).
[23] E. Santiso and E. A. Muller, Mol. Phys. **100**, 2461 (2002).
[24] M. Wackenhut and H. Herrmann, Phys. Rev. E **68**, 041303 (2003).
[25] H. J. Herrmann, R. M. Baram, and M. Wachenhut, Braz. J. Phys. **33**,591 (2003).
[26] V. N. Nikolaevskiy, *Geomechanics and Fluidodynamics* (Kluwer, Dordrecht, 1996), p.7.
[27] S. P. Timoshenko and J. N. Goodier, *Theory of Elasticity* (McGraw-Hill International Editions, 1970), p.11.
[28] S. C. Cowin, Powder Technol. **9**, 61 (1974).